Feedback between residual circulations and sediment distribution in highly turbid estuaries: An analytical model

S.A. Talke[a],[*],[1], H.E. de Swart[a], H.M. Schuttelaars[b]

[a]*Institute for Marine and Atmospheric Research, Utrecht University, Princetonplein 5, 3584 CC Utrecht, The Netherlands*
[b]*Delft Institute of Applied Mathematics/Mathematical Physics, Delft University of Technology Mekelweg 4, P.O. Box 5031, 2600 GA Delft, The Netherlands*

Abstract

Motivated by field studies of the Ems estuary which show longitudinal gradients in bottom sediment concentration as high as $O(0.01\,\text{kg/m}^4)$, we develop an analytical model for estuarine residual circulation based on currents from salinity gradients, turbidity gradients, and freshwater discharge. Salinity is assumed to be vertically well mixed, while the vertical concentration profile is assumed to result from a balance between a constant settling velocity and turbulent diffusive flux. Width and depth of the model estuary are held constant. Model results show that turbidity gradients enhance tidally averaged circulation upstream of the estuarine turbidity maximum (ETM), but significantly reduce residual circulation downstream, where salinity and turbidity gradients oppose each other. We apply the condition of morphodynamic equilibrium (vanishing sediment transport) and develop an analytical solution for the position of the turbidity maximum and the distribution of suspended sediment concentration (SSC) along a longitudinal axis. A sensitivity study shows great variability in the longitudinal distribution of suspended sediment with the applied salinity gradient and six model parameters: settling velocity, vertical mixing, horizontal dispersion, total sediment supply, fresh water flow, and water depth. Increasing depth and settling velocity move the ETM upstream, while increasing freshwater discharge and vertical mixing move the ETM downstream. Moreover, the longitudinal distribution of SSC is inherently asymmetric around the ETM, and depends on spatial variations in the residual current structure and the vertical profile of SSC.
© 2007 Elsevier Ltd. All rights reserved.

Keywords: Gravitational circulation; Gravity currents; Turbidity currents; Estuarine turbidity maximum; Morphodynamics; Sediment dynamics; Fluid mud; Ems estuary

1. Introduction

Many estuaries (e.g., the Ems, Humber, Gironde) have extremely large sediment concentrations at their turbidity maximum (estuarine turbidity maximum, ETM). Suspended sediment concentrations (SSCs) and fluid mud of greater than $10\,\text{kg/m}^3$ have been reported for the Gironde and Humber estuaries (Abril et al., 1999; Uncles et al., 2006). At such large concentrations, sediment significantly affects the vertical density structure, causing stratification and a reduction of mixing (Munk and Anderson, 1948; Kineke et al., 1996; van der Ham and Winterwerp, 2001; Winterwerp, 2001), thereby affecting, for example, tidal propagation (Gabioux et al., 2005).

Previous model studies on the formation of ETM have treated suspended sediment as a passive material (not affecting the flow directly) whose distribution along an estuary is set by a balance between convergent residual circulation and the spreading effects of horizontal dispersion. For example, the tidally averaged numerical model of Festa and Hansen (1978) produces a convergence zone of sediment from the balance between gravitational circulation (Hansen and Rattray, 1965; Officer, 1976) and freshwater discharge. More recent research has highlighted the importance of tidally varying processes on the formation of residual flows and sediment fluxes (Simpson

*Corresponding author.

E-mail addresses: s.a.talke@phys.uu.nl (S.A. Talke),
h.e.deswart@phys.uu.nl (H.E. de Swart),
H.M.Schuttelaars@ewi.tudelft.nl (H.M. Schuttelaars).
[1]Present address. Civil & Environmental Engineering, University of Washington, 201 More Hall, Box 352700 Seattle, WA 98195-2700, USA.

et al., 1990; Geyer, 1993; Jay and Musiak, 1994; Burchard and Baumert, 1998).

The direct effect of large sediment concentrations on the longitudinal density structure (and hence residual current patterns) has not been investigated in estuaries. Dense fluid mud layers and down-slope turbidity-driven gravity flows have been modelled on the continental shelf (e.g., Parker et al., 1986; Scully et al., 2002; Friedrichs and Wright, 2004). Although some numerical models have modelled fluid mud in estuaries (Le Hir et al., 2001a; Guan et al., 2005), they have not explicitly investigated the dynamic effect of longitudinal gradients in sediment. In this paper, we show that elevated sediment concentrations found in highly turbid estuaries significantly alter the along-estuary density structure. Using an analytical model based on the gravitational circulation model of Hansen and Rattray (1965), we show that the resulting gradients of sediment concentration then produce turbidity-driven flows.

We also develop a tidally averaged model for the distribution of suspended sediment around the turbidity maximum for basins with both small and large SSCs. Using the analytical solution, we investigate the changes to the position and shape of the longitudinal profile of suspended sediment as input parameters such as the salinity structure, freshwater discharge, and total amount of sediment available for resuspension are altered. In Section 2 we describe the measurements that motivate the inclusion of longitudinal sediment gradients in a model of tidally averaged circulation, which is introduced in Section 3. Results are presented in Section 4, followed by a discussion (Section 5) and conclusions.

2. Observational background

The Ems-Dollard estuary is a partially mixed, mesotidal estuary (tidal range ∼3.5 m) located on the border of the Netherlands and Germany (see Fig. 1). Between the North Sea barrier islands and the harbor town of Emden the water depth averages between 10 and 20 m, while much of the remaining 53 km to the tidal weir in Herbrum (100 km in our coordinate system) is maintained at a navigable depth of ∼7 m. Tidal flats cover ∼50% of the estuary, and ∼80% of the Dollard sub-basin. Approximately 90% of the freshwater input into the estuary comes from the Ems River with an average freshwater discharge of ∼100 m³/s (de Jonge, 1992).

Between February 2005 and October 2006, we conducted nearly monthly cruises along the axis of the estuary (see Fig. 1). In addition, experiments have been conducted over a tide at selected cross-sections near the town of Pogum (see Fig. 1). For this paper, we refer to longitudinal data that were collected on September 28, 2005 and August 2, 2006, as well as cross-sectional data collected on February 15, 2005. Moreover, we also use long-term monitoring data collected by the German state of Niedersachsen, the NLWKN, to estimate the tidally averaged salinity gradient (locations are displayed with an 'X' in Fig. 1).

During longitudinal cruises, salinity and turbidity were measured by an Aanderaa RCM-9 by pumping surface water through an on-board flow-through system. Vertical profiles of turbidity, salinity and depth were made with an RBR-XR620, a conductivity–temperature–depth (CTD) profiler with an attached optical backscatter sensor (OBS). Data were logged internally and measured continuously at 6 Hz, and casts were made every 1–3 km (longitudinal cruise) or at varying phases of the tide (cross-sectional cruise). Water samples were either pumped or grabbed from near the CTD instrument at known times and depths, and were processed in a laboratory to obtain sediment concentrations. We calibrated the OBS data using ∼150 water samples from the February 14th/February 15th experiment in both the linear and non-linear range using the method of Kineke and Sternberg (1992). Moreover, conductivity values were re-measured in each water sample
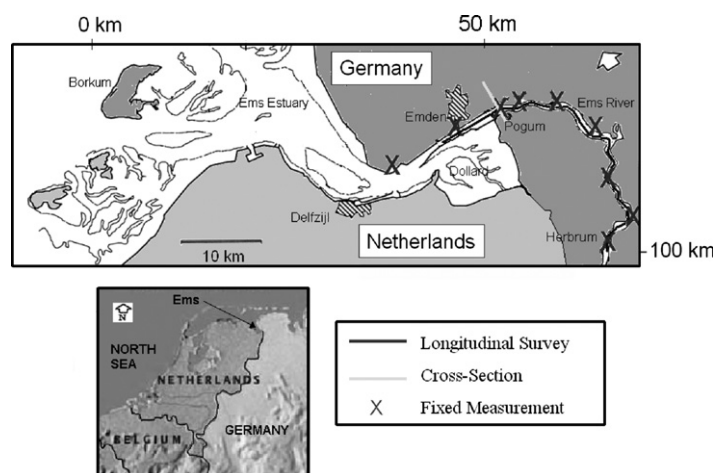
Fig. 1. Map of the Ems/Dollard estuary. The dark line indicates the location of the longitudinal surveys on September 28, 2005 and August 2, 2006 between 45 and 100 km and the light-colored line indicates the location of cross-sectional measurements over a tide on February 15, 2006 at 53 km (near Pogum). The nine fixed-point measurements shown with an X were used to determine the tidally averaged salinity gradient (data courtesy of NLWKN in Germany).
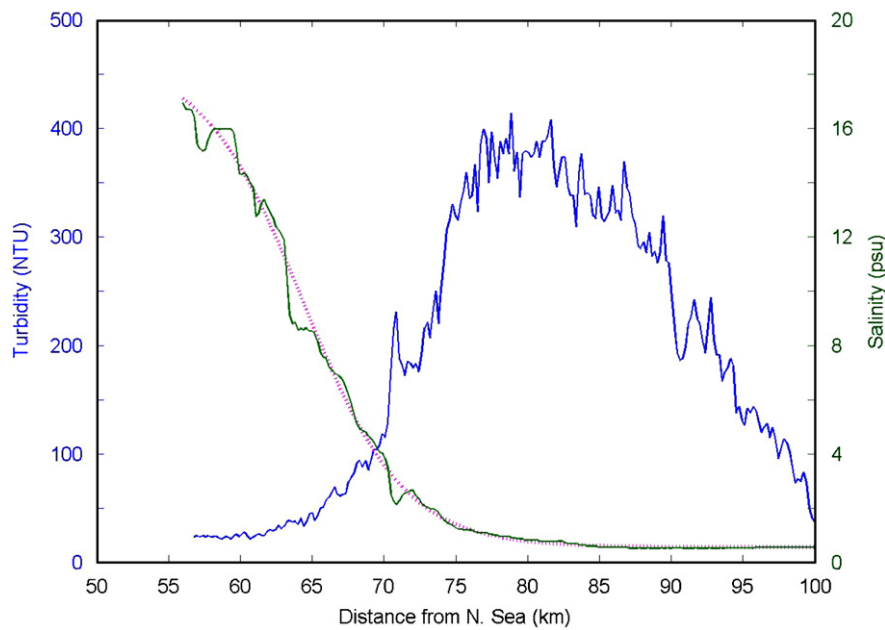
Fig. 2. Observations of the longitudinal distribution of turbidity (NTU) and salinity (psu) along the longitudinal axis of the Ems estuary on September 28, 2005. A hyperbolic tangent (dotted line) fits the salinity profile (light-colored, green line) well.
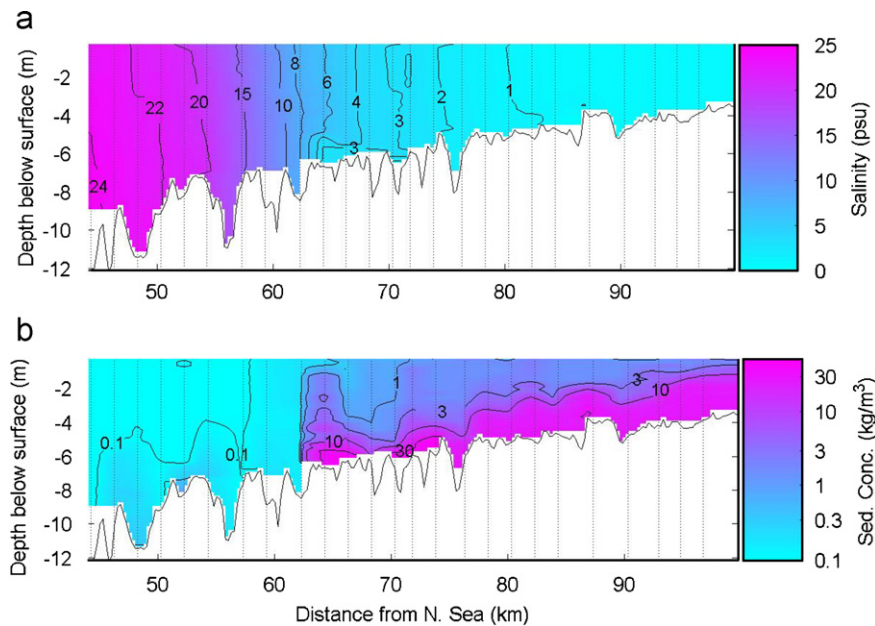

Fig. 3. Longitudinal distribution of salinity (a) and suspended sediment concentration (b) along the Ems estuary during the ebb tide on August 2, 2006. The 25 OBS/CTD casts are represented by vertical dotted lines. The cruise began just downstream of Emden (45 km) approximately 4 h before low-water (LW) slack, and ended in Herbrum (100 km) at LW slack.

after sediment had settled to the bottom, to ensure that the measured conductivity was not affected by high sediment concentrations. Results show that the variation in conductivity at different SSCs is not significant (<0.5 psu).

2.1. Results

Fig. 2 shows the variation in surface salinity and turbidity (1–2 m below surface) along the longitudinal axis

of the Ems estuary on September 28, 2005. Note that the measurements were taken approximately at the same tidal phase during the ebb tide. As the boat travelled upstream, salinity values decrease from about 17 psu to a minimum of about 0.5 psu in the upstream portion of the estuary. By contrast, turbidity begins to increase steeply at about 65 km from the North Sea, rising to a maximum at ~78 km, and then decreasing slowly back towards background conditions. The profile of turbidity is asymmetric; downstream
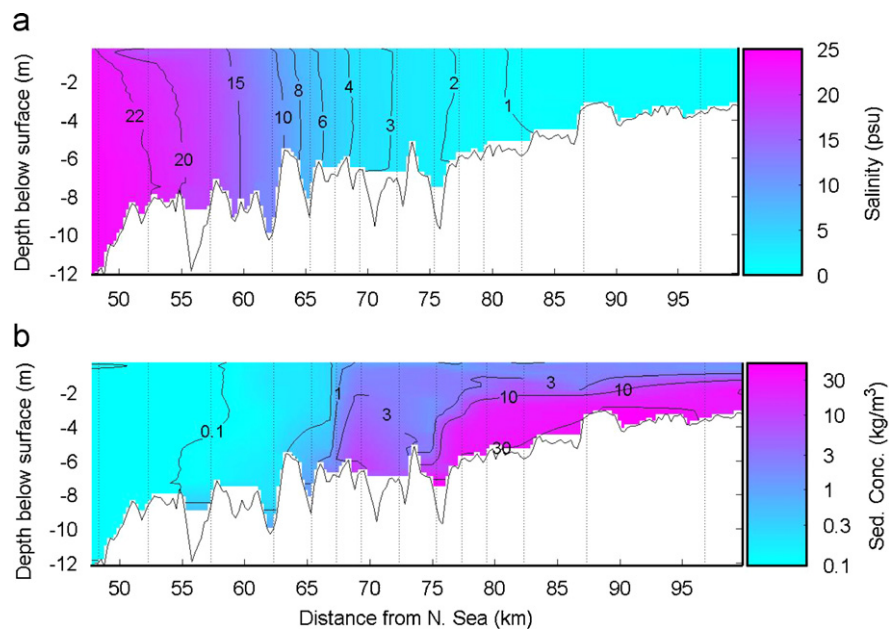
Fig. 4. Longitudinal distribution of salinity (a) and suspended sediment concentration (b) along the Ems estuary during the flood tide on August 2, 2006 (return trip to Emden). The results are concatenated from 14 vertical profiles of salinity and optical backscatter, which are shown with dotted lines. Differences in water depth and bathymetry between Fig. 3 and this figure reflect differences in ship course and tidal stage. The return cruise started ∼3.5 h before high-water (HW) slack (∼2 h after LW), and ended in Emden ∼30 min after HW slack.

of the ETM, turbidity measurements are greater than 100 NTU (practical turbidity units) for ∼10 km, while upstream this level is exceeded for ∼20 km. We note that a hyperbolic tangent can be fit to the salinity profile.

Fig. 3 provides a snapshot of both the vertical and longitudinal distribution of SSC and salinity during the ebbing tide on August 2, 2006, after a month of low flow conditions ($< 30 \, m^3/s$). Salinity is well mixed over most of the estuary during this tidal phase, except for a small area between 64 and 70 km in which near-bottom salinity (corresponding with large SSC) is less than surface salinity. In the deeper portion of the estuary, sediment concentrations are quite small throughout the water column and are generally less than $0.1 \, kg/m^3$. Further upstream, a sudden increase in the sediment concentration occurs between 62 and 64 km. Near the bottom ($< 2 \, m$ from the bed), fluid mud concentrations of between 10 and $80 \, kg/m^3$ are found between 64 and 100 km. The maximum horizontal gradient in near-bed sediment concentration during this cruise is on the order of $O(0.01 \, kg/m^4)$, and coincides with large longitudinal salinity gradients of $O(0.001 \, psu/m)$ at the toe of the salt wedge. Interestingly, no distinct turbidity maximum occurs in the bottom concentration, although the largest absolute values occur between 70 and 75 km. Rather, the 36 km stretch from 64 km to the tidal weir at 100 km is a contiguous zone of high bottom sediment concentrations with pools of fluid mud 1–2 m thick covering the bed.

Fig. 4 shows a snapshot of the vertical and longitudinal distribution of SSC during the flood tide on August 2, 2006, on the return trip from Herbrum to Emden. Similar gradients in the longitudinal gradient of SSC are observed

as during the ebb, $O(0.01 \, kg/m^4)$, though the location of the maximum gradient is shifted upstream by ∼10 km. Compared to the ebb, the stronger flood currents have mixed sediment higher in the water column. Throughout the domain, salinity is well mixed in the vertical direction during this tidal phase. The comparison of Figs. 3 and 4 shows that large sediment concentration gradients are present during both the flood and ebb tides, and that salinity is well mixed or partially mixed over most of the measured domain.

The large bottom sediment concentrations observed during the longitudinal cruise of August 2, 2006 are echoed in the results of fixed measurements taken at ∼54 km (46 km from weir) over two tidal periods on February 14th, 2006 and February 15, 2006 (Fig. 5). Fig. 5a shows a scatter plot of SSC vs. depth found from water samples, along with the average SSC found from 21 CTD/OBS casts. Sediment concentrations range from ∼$0.3 \, kg/m^3$ at the surface to greater than $70 \, kg/m^3$ at the bed. Variations are also observed with tidal phase, with SSC being mixed higher into the water column during the more energetic flood tide.

Each profile of concentration $C(z)$ found from the 21 OBS/CTD casts is fitted to an exponential profile of $C(z) = C_b \exp\{-r(z + H)\}$, where C_b is the bottom concentration, z is the vertical coordinate measured upwards from the surface, H is the water depth, and r is a decay coefficient. Fig. 5b shows that the observed variation in the decay coefficient r between different casts ranges from 0.5 to $1.1 \, m^{-1}$, with the smallest values observed during the energetic flood. Thus, to a first order, the vertical distribution of suspended sediment (even in this highly
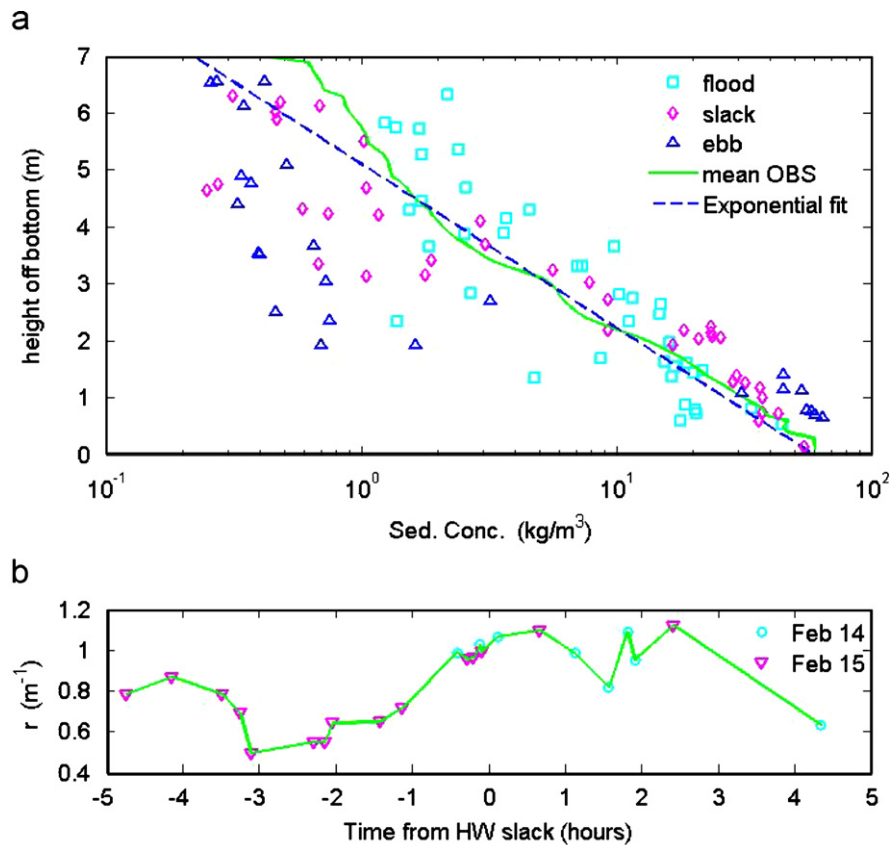
Fig. 5. Vertical distribution of suspended sediment concentration (a) and the tidal variation of the exponential fitting parameter r (b) found from 21 OBS/CTD casts and 103 water samples on February 14th and February 15th, 2006. Measurements occurred on the shipping channel near Pogum, about 54 km from the North Sea (46 km from the tidal weir). Water samples collected during the flood, slack period, and ebb are denoted by squares, diamonds, and triangles. High-water slack lags high water by ~30 min. The fitting parameter r occurs in the equation $C(z) = C_b \exp\{-r(z+H)\}$, and ranges in value from r~0.5 to 1.1 m^{-1}. The goodness of fit to the 21 OBS casts ranged from $R^2 = 0.56$ to 0.97, with a mean of $R^2 = 0.8$. The average of 21 optical backscatter profiles (solid green line) and an exponential fit (dashed blue line) with $r = 0.8$ is shown in (a).

stratified environment) follows an exponential profile. An exponential profile with the mean decay coefficient of $r = \sim 0.8$ m^{-1} is shown in Fig. 5a, and shows a reasonable fit to the data. The scatter of the sediment concentration data around the mean exponential profile attests to variation in SSC between different casts.

These experimental results show that SSCs can significantly alter the density structure of an estuary, both in the vertical and longitudinal direction. In particular, the sediment concentration gradients downstream of the ETM are particularly sharp and coincide spatially with significant salinity gradients. These observations lead directly to the analytical model, which is the focus of this paper.

3. Model

The system of tidally averaged equations presented below is solved analytically to obtain an equilibrium distribution of sediment and tidally averaged circulation along the longitudinal axis of an estuary. The origin of the Cartesian coordinate system is set at the water surface, with the z-axis pointing vertically upward and the positive longitudinal direction x going into the estuary (upstream).

The setup closely follows the classic formulation of gravitational circulation (Hansen and Rattray, 1965), which assumes that salinity (s) is well mixed in the vertical direction and that eddy viscosity (A_v) is constant. The Boussinesq approximation is applied, and salinity varies gradually in the horizontal direction. We also assume that the height variation induced by the surface slope is insignificant relative to the depth (rigid-lid assumption). Pressure is assumed to be atmospheric at the water surface. A synopsis of assumptions is given in Fig. 6.

Following Hansen and Rattray (1965), we define gravitational circulation as a balance between density-induced (baroclinic) pressure gradients and the constant (barotropic) pressure gradient induced by the spatially varying surface slope $d\eta/dx$. The equations are

$$0 = -g \int_z^0 \frac{\partial \rho}{\partial x} dz' - g\rho_o \frac{d\eta}{dx} + \frac{\partial}{\partial z}\left\{ \rho_o A_v \frac{\partial u}{\partial z} \right\}, \tag{1}$$

$$\int_{-H}^0 ub\, dz = Q. \tag{2}$$

Mathematically, the horizontal momentum equation is a balance between the longitudinal pressure force (first and
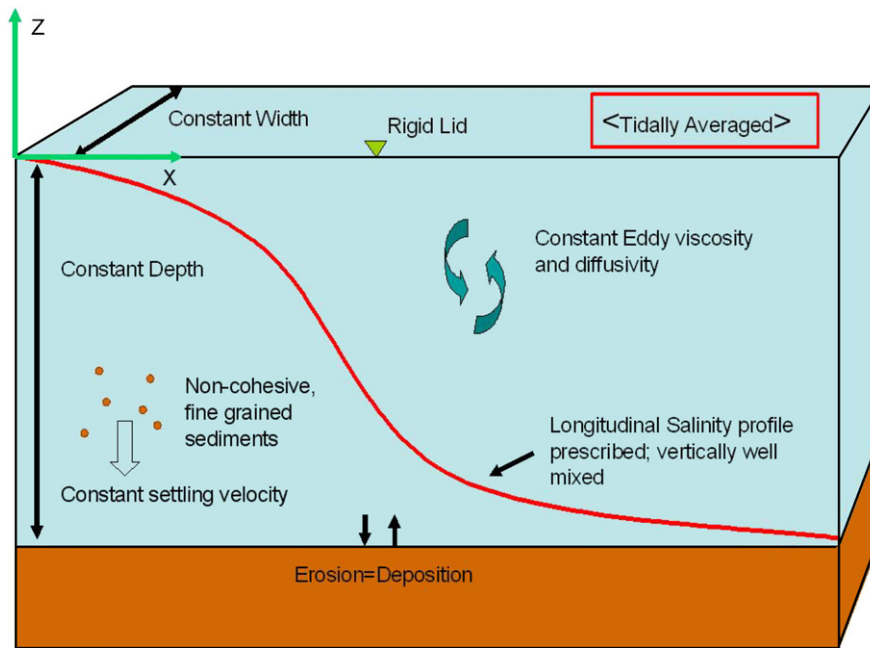
Fig. 6. Assumptions made in the steady channel model.

second terms on the right-hand side of Eq. (1)) and the internal friction force (third term on the right-hand side of Eq. (1)). Using continuity and the rigid-lid assumption, we require that the total flow of water through a cross-section of width b and height H is equal to the prescribed freshwater flow, Q (Eq. (2)). The freshwater discharge Q is a negative quantity in our coordinate system. To solve these equations, we apply the no-slip condition at the bed and assume that no stress is applied at the water surface:

$$u|_{z=-H} = 0, \tag{3}$$

$$\rho_o A_v \frac{\partial u}{\partial z}\bigg|_{z=0} = 0. \tag{4}$$

Furthermore, we define the density ρ as a linear function of both the salinity $s(x)$ and the SSC $C(x,z)$,

$$\rho(x,z) = \rho_o + \beta s(x) + \gamma C(x,z). \tag{5}$$

Here, β is $\sim 0.83\,\mathrm{kg/m^3/psu}$ and $\gamma = (\rho_s - \rho_o)/\rho_s \sim 0.62$ is the relative density of suspended sediment (ρ_s) to water (ρ_o). All sediment is assumed to be fine-grained, non-cohesive, and consist of a single grain size. We consider particles with a density of $2650\,\mathrm{kg/m^3}$ and water with a density of $\rho_o \sim 1000\,\mathrm{kg/m^3}$. The tidally averaged longitudinal salinity distribution $s(x)$ is prescribed diagnostically as a hyperbolic tangent profile along the axis of the estuary and depends upon the four parameters S_b, S_*, x_c, x_L:

$$s(x) = S_b + 0.5S_*\left\{1 - \tanh\left(\frac{x - x_c}{x_L}\right)\right\}, \tag{6}$$

where S_b is the salinity as x approaches infinity, S_* is the salinity scale, x_c defines the position of the maximum salinity gradient, and x_L defines the length scale over which salinity varies.

Next, using scaling arguments, it follows in leading order that the vertical distribution of suspended sediment is a balance between the settling of sediment and its upwards diffusion by turbulent mixing (more detail is given in the electronic supplement (Appendix B)):

$$\frac{\partial}{\partial z}\left[w_s C + K_v \frac{\partial C}{\partial z}\right] = 0, \tag{7}$$

where w_s is the constant settling velocity of sediment and K_v is the eddy diffusivity. For simplicity, we set K_v equal to A_v. At the top and bottom boundary we assume in leading order that no flux of sediment occurs,

$$\left\{w_s C + K_v \frac{\partial C}{\partial z}\right\}\bigg|_{z=0, z=-H} = 0. \tag{8a,b}$$

To solve for the unknown bottom concentration $C_b(x, z = -H)$, we apply the condition of morphodynamic equilibrium to the model, which states that the vertically integrated fluxes of sediment vanish at each location during equilibrium conditions. For a tidally averaged model, this reduces to a balance between the horizontal advection and the diffusion of sediment, i.e.,

$$\int_{-H}^{0}\left\{uC - K_h \frac{\partial C}{\partial x}\right\}\mathrm{d}z = 0, \tag{9}$$

where K_h is the tidally averaged longitudinal diffusion coefficient. More information is given in the electronic supplement (Appendix B); the concept of morphodynamic equilibrium is also discussed in Friedrichs et al. (1998) and Huijts et al. (2006). To close the model, we define the

average amount of bottom sediment available for resuspension over a channel of length L by the parameter c_*,

$$c_* = \frac{1}{L} \int_0^L C_b(x)\, \mathrm{d}x. \tag{10}$$

Hence, the total mass of sediment in the domain of length L is constrained by c_*. From this set of equations (Eqs. (1)–(10)) we can derive an analytical solution for residual circulation and the equilibrium distribution of sediment concentration as a function of the salinity profile $s(x)$ and seven independent parameters: H, A_v, Q, w_s, K_h, c_*, and L.

3.1. Salinity- and turbidity-induced circulation

To obtain an estimate of tidally averaged circulation patterns for a given distribution of SSC and salinity, we first solve Eq. (7) to obtain the vertical distribution of sediment concentration as a function of the bottom sediment concentration $C_b(x)$,

$$C = C_b \exp\{-Pe_v(\zeta + 1)\}. \tag{11}$$

where $\zeta = z/H$ is the non-dimensional vertical coordinate and $Pe_v = w_s H/K_v$ is the Peclet number for SSC. Comparison of Eq. (11) with the profile fitted to data in Fig. 5 shows that the fitting parameter r is the ratio of settling velocity to vertical eddy diffusivity, i.e., $r = w_s/K_v$.

Integrating the momentum equation (Eq. (1)) twice with respect to z gives an expression for the velocity u in terms of the longitudinal salinity gradient $\mathrm{d}s/\mathrm{d}x$, the bottom turbidity gradient $\mathrm{d}C_b/\mathrm{d}x$, and the surface slope $\mathrm{d}\eta/\mathrm{d}x$. The surface slope is found by applying Eq. (2) (mass balance of water). After substituting the expression for $\mathrm{d}\eta/\mathrm{d}x$ and simplifying, the residual velocity u is expressed as follows:

$$u = \frac{g\beta H^3}{48\rho_o A_v} k_1(\zeta) \frac{\mathrm{d}s}{\mathrm{d}x} + \frac{g\gamma H^3}{48\rho_o A_v} k_2(\zeta, Pe_v) \frac{\mathrm{d}C_b}{\mathrm{d}x}$$
$$+ \frac{3Q}{2bH}\{1 - \zeta^2\}. \tag{12}$$

Eq. (12) specifies the residual circulation as a function of ζ, Pe_v, the salinity gradient ($\mathrm{d}s/\mathrm{d}x$), and the gradient in bottom sediment concentration $\mathrm{d}C_b/\mathrm{d}x$, provided that the assumptions in the model are met. The functions $k_1(\zeta)$ and $k_2(\zeta, Pe_v)$ are defined in Appendix A and describe the dimensionless vertical structure of salinity-gradient-driven currents and turbidity-gradient-driven currents, respectively. If k_2 or $\mathrm{d}C_b/\mathrm{d}x$ in Eq. (12) is set to zero, the gravitational circulation model of Hansen and Rattray (1965) is recovered.

3.2. Solution for near-bed concentration

Eq. (12) describes the tidally averaged currents that occur given the observed gradients of turbidity and salinity in an estuary. However, the solution assumes a priori knowledge of the longitudinal gradients in sediment concentration. To obtain an equilibrium solution for the distribution of sediment (and hence the concentration gradient), we next apply the condition of morphodynamic equilibrium (Eq. (9)). After substituting the expression for sediment concentration (Eq. (11)) and velocity (Eq. (12)) into Eq. (9) and integrating over the vertical, we obtain a differential equation for the bottom sediment concentration $C_b(x)$,

$$\underbrace{\frac{-T_s g\beta H^3}{48\rho_o A_v} \frac{\mathrm{d}s}{\mathrm{d}x} C_b(x)}_{F_s} + \underbrace{\frac{3T_Q Q}{2bH} C_b(x)}_{F_Q}$$
$$- \underbrace{\frac{T_T g\gamma H^3}{48\rho_o A_v} C_b(x) \frac{\mathrm{d}C_b}{\mathrm{d}x}}_{F_T} - \underbrace{T_K K_h \frac{\mathrm{d}C_b}{\mathrm{d}x}}_{F_K} = 0. \tag{13}$$

The terms F_S, F_Q, F_T, and F_K represent the vertically integrated sediment flux (sediment transport) due to salinity gradients, freshwater discharge, turbidity-gradient-driven currents, and longitudinal dispersion, respectively. The parameters T_S, T_T, T_Q, and T_K are functions of $Pe_v = w_s H/K_v$ (sediment Peclet number) and are defined in Appendix A.

Eq. (13) is integrated with respect to x to yield an implicit solution for the distribution of bottom SSC:

$$C_b(x) = A_1 \exp\left[-\frac{1}{T_K K_h} \left\{ T_s \frac{g\beta H^3}{48\rho_o A_v} s(x) \right. \right.$$
$$\left. \left. - T_Q \frac{3Q}{2bH} x + T_T \frac{g\gamma H^3}{48\rho_o A_v} C_b(x) \right\} \right], \tag{14}$$

where A_1 is a parameter that follows from Eq. (10) and depends on the parameter c_* (average bottom SSC).

The sediment distribution in our model is thus a function of the prescribed longitudinal salinity distribution (Eq. (6)) and of the parameters c_*, H, w_s, K_v, A_v, K_h, L and $q = Q/b$ (width averaged freshwater discharge). The solution to the implicit equation is found by first finding a solution for A_1 in the limiting case in which the contribution of turbidity currents are neglected ($F_T = 0$). Using the initial solution for A_1, a root finding algorithm is next used to solve for

Table 1
Default parameters used to calculate circulation and the equilibrium distribution of sediment

S_* (psu)	S_b (psu)	x_L (m)	x_c (m)	A_v (m^2/s)	K_v (m^2/s)	w_s (m/s)	H (m)	q (m^2/s)	K_h (m^2/s)	c_* (kg/m^3)
25.1	0.3	12,500	53,000	0.001	0.001	0.0008	7	-0.01	100	1

S_* is the salinity scale, S_b is the salinity as $x \to \infty$, x_L scales the salinity gradient, x_c is the location of the maximum salinity gradient relative to the seaward boundary, A_v = eddy viscosity, K_v = eddy diffusivity, w_s = settling velocity, H = depth, K_h = horizontal dispersion coefficient, and c_* is the average bottom sediment concentration. Note that the width-averaged discharge $q = Q/b$ is negative in our coordinate system.

$C_b(x)$ in Eq. (14). The calculated value of $C_b(x)$ is next used to re-estimate A_1, which is then used to re-estimate $C_b(x)$ (Eq. (14)). This is repeated until the solution for the sediment concentration $C_b(x)$ and the constant A_1 have converged.

4. Results

The solutions presented in Sections 3.1 and 3.2 present two related but distinct results. Section 3.1 describes the circulation that occurs when significant gradients in both salinity and sediment concentration occur, while Section 3.2 describes a solution for the equilibrium distribution of bottom SSC at the turbidity maximum. Therefore, we separate the results of these two distinct (but related) facets of the model. Unless otherwise specified, we use the default parameter values listed in Table 1, which reflect typical values found in mesotidal estuaries such as the Ems. The four parameters of the salinity profile are found by making a least-squares fit to tidally averaged salinity data from the long-term monitoring stations on the Ems River, and are typical of the low discharge conditions observed in the summer of 2005.

4.1. Density-driven currents

The expression for density-driven circulation (Eq. (12)) is used to investigate the vertical current structure both upstream and downstream of the turbidity maximum (Fig. 7), independent of whether the system is in morphodynamic equilibrium. The values of the salinity gradient and the turbidity gradient are based on observed salinity and turbidity gradients in the Ems estuary. Downstream of the ETM we apply a salinity gradient of -5×10^{-4} psu/m, while upstream the salinity gradient decreases and is on the order of -1×10^{-4} psu/m. Similarly, the gradient in bottom sediment concentration is specified as 0.008 kg/m^2 in the downstream direction, and is assumed to be -0.001 kg/m^2 in the upstream direction. River inflow Q is neglected.

Upstream of the ETM, the residual currents induced by salinity and turbidity gradients both act in the upstream direction (Fig. 7a). Thus, although both the turbidity and the salinity gradients are less than downstream of the ETM, they act together to magnify the overall upstream flow near the bottom and the seaward flow at the surface. Compared to salinity-gradient-driven flow, the maximum upstream current from turbidity gradients occurs closer to the bed. Downstream of the ETM, turbidity currents and salinity-induced currents act in opposing directions, and the combined magnitude of the residual circulation is reduced (see Fig. 7b). Compared to the case of salinity-gradient-only flow, the combined landward flow is shifted upwards in the water column. Moreover, for the parameter values chosen, the combined residual current shown in Fig. 7b is characterized by a three-layer circulation pattern: turbidity gradients drive seaward flow near the bottom, salinity gradients drive landward flow in a middle layer, and the barotropic pressure gradient drives a seaward return flow in the top layer. Such a three-layer circulation
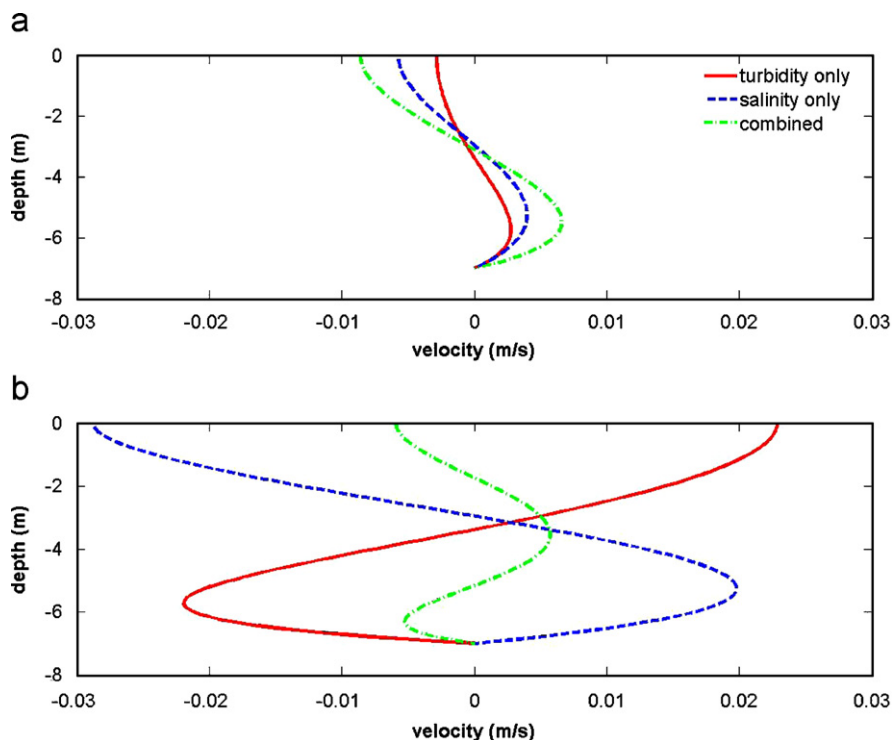

Fig. 7. Example of residual current structure upstream (a) and downstream (b) of the ETM from turbidity currents (solid), salinity-driven flow (dark, dashed) and the combined flow (light shade, dash–dot). The bottom is at a depth of 7 m below the surface.
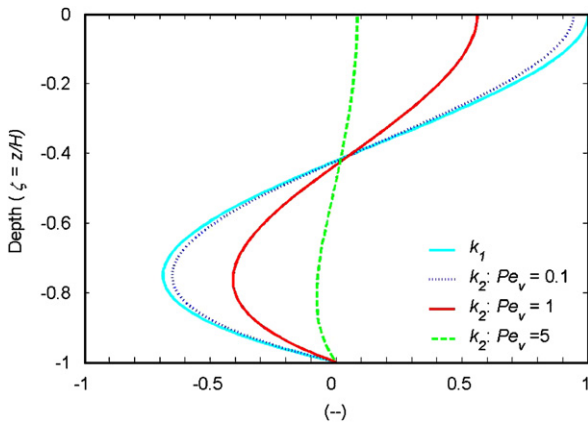
Fig. 8. Plot of the dimensionless vertical structure of circulation due to salinity gradients (k_1) and turbidity gradients (k_2), which is shown for three values of the sediment Peclet number Pe_v.

can only occur when the order of magnitude of turbidity currents are the same as salinity-driven currents (see Eq. (12)), and implies that $(\gamma k_2 \, dC_b/dx)/(\beta k_1 \, ds/dx) = O(1)$.

The vertical distribution of SSC, which depends on the sediment Peclet number Pe_v (see Eq. (11)), affects turbidity-gradient-driven circulation through the function $k_2(\zeta, Pe_v)$ in Eq. (12). Fig. 8 compares the dimensionless vertical structure of currents caused by salinity gradients and turbidity gradients, as defined, respectively, by the functions $k_1(\zeta)$ and $k_2(\zeta, Pe_v)$ in Appendix A. For small Pe_v (e.g., $Pe_v = 0.1$), the vertical profile of k_2 approaches the vertical profile caused by salinity gradients, k_1. As Peclet number increases, the near-bed maximum of k_2 is shifted towards the bed, and the magnitude decreases (Fig. 8); between $Pe_v = 0.1$ and $Pe_v = 100$, the typical magnitude decreases by four orders of magnitude. Therefore, the magnitude of turbidity currents decrease as Pe_v increases, and are negligible for large Pe_v (see Eq. (12)).

This result can be understood by scaling the time for a particle to settle through a water column ($\tau_{settling}$) as H/w_s, and the time scale for mixing through the water column (τ_{mixing}) as H^2/K_v. Hence we can rewrite the Peclet number as $Pe_v = (w_s/H)(H^2/K_v) = \tau_{mixing}/\tau_{settling}$. When the time scale for settling is small in comparison to the mixing time scale (Pe_v large), turbidity currents are greatly suppressed. Suspended sediments are concentrated close to the bed (Pe_v large), and the no-slip condition (Eq. (3)) enforces zero velocity and reduces k_2. When the time scale for mixing the water column is small compared to the settling time (Pe_v small), SSC is shifted upwards in the water column. As a result, the effect of the no-slip condition is decreased and the turbidity currents are enhanced. For small Pe_v, suspended sediment approaches uniformly mixed conditions, and the vertical profile of k_2 approaches k_1.

4.2. Equilibrium distribution of sediment

An example of the equilibrium distribution of bottom SSC (Eq. (14)) is shown in Fig. 9a for small ($1\,kg/m^3$),

intermediate ($10\,kg/m^3$), and large ($200\,kg/m^3$) values of the average bottom concentration, c_*. To compare variations to the shape of the sediment distribution, each profile is normalized by the value of SSC at its turbidity maximum. The longitudinal axis is divided by $x_s = x_c + x_L = 65.5 \times 10^3\,m$, which is an approximate scale for the salinity intrusion into the Ems estuary during low freshwater discharge conditions.

As c_* becomes larger, the spread of SSC relative to its maximum value (C_b/C_{max}) increases, particularly in the upstream direction. However, the position of the turbidity maximum remains constant, indicating that c_* only affects the distribution—but not the maximum—of suspended sediment. The distribution of SSC is explained by considering the four components of sediment transport defined by Eq. (13) for different values of c_* (Fig. 9b–g). For comparison, we normalize each component of transport by the maximum transport due to salinity gradients (F_S) and present the relative magnitude over the model domain on a logarithmic scale. Arrows indicate that the transport from gravitational circulation (F_S) is directed upstream and that the transport from freshwater discharge (F_Q) is directed downstream (Fig. 9b, d, and f). The transport from dispersion (F_K) and turbidity currents (F_T) oppose the turbidity gradient dC_b/dx, and hence serve to spread sediment away from the maximum at $x/x_s \sim 1.3$ (Fig. 9c, e, and g). The sum of the four transport components—as defined by Eq. (13)—is zero at each longitudinal position.

As shown in Fig. 9b, d, and f, downstream sediment transport from freshwater discharge (F_Q) dominates over upstream sediment transport from the salinity gradient (F_S) at both the landward and seaward limit of the model domain. In between, from $x/x_s \sim 0.35$ to $x/x_s \sim 1.3$, F_S dominates over F_Q. At $x/x_s \sim 1.3$, the convergence of sediment transport from gravitational circulation (F_S) and freshwater discharge (F_Q) form the classical ETM (Festa and Hansen, 1978). The sediment transport rate F_S and F_Q also balance each other at $x/x_s \sim 0.35$, but are oriented in opposite directions. Hence, the divergence of vertically integrated fluxes F_S and F_Q at $x/x_s \sim 0.35$ describes a turbidity minimum.

The relative importance of sediment transport from turbidity currents (F_T) compared to dispersion (F_K) is investigated in Fig. 9c, e, and g. For the standard parameter values presented in Table 1, dispersive transport (F_K) dominates over transport from turbidity currents (F_T). As the sediment supply increases ($c_* = 10\,kg/m^3$), transport from turbidity currents is still smaller than dispersive transport (Fig. 9e), but has a corrective effect on the distribution of SSC (Fig. 9a). At extremely large values of c_* (or small values of dispersion), turbidity currents dominate the spread of sediment away from the turbidity maximum (Fig. 9g).

Fig. 10a shows the effect of varying settling velocity (and hence sediment Peclet number Pe_v) on the distribution of bottom SSC. As settling velocity is increased, the turbidity
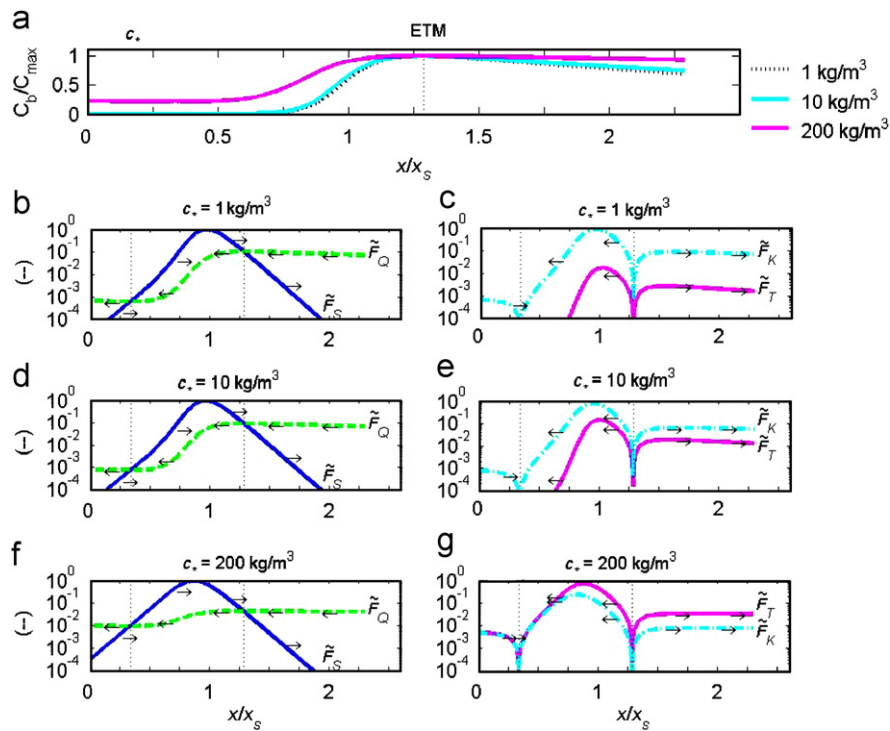
Fig. 9. Modelled profile of SSC for different values of c_* (a) and normalized sediment transport rates due to the salinity gradient ($\tilde{F}_s$, solid line in (b), (d), and (f)), freshwater discharge ($\tilde{F}_Q$, dashed line in (b), (d), and (f)), turbidity currents ($\tilde{F}_T$, solid line in (c), (e), and (g)), and dispersion ($\tilde{F}_K$, dash–dot line (c), (e), and (g)), where the tilde indicates normalized magnitudes. The x-axis is normalized by a salt intrusion length scale, $x_s = x_c + x_L \sim 65.5 \times 10^3$ m, while each profile of SSC is normalized by the value at the ETM. The sediment transport rates are normalized by the maximum value of F_S, and presented on a logarithmic scale. Arrows show the direction of each transport component. The locations at which transport rates from freshwater discharge F_Q and salinity gradients F_S, are equal are denoted by a vertical dashed line. The ETM for all three cases occurs at $x/x_s = 1.29$, and the model domain runs from $x/x_s = 0$ to $x/x_s = 2.3$. The maximum value of the sediment transport rate F_S is 0.002, 0.022, and 0.72 kg m/s for (b), (d), and (e), respectively.
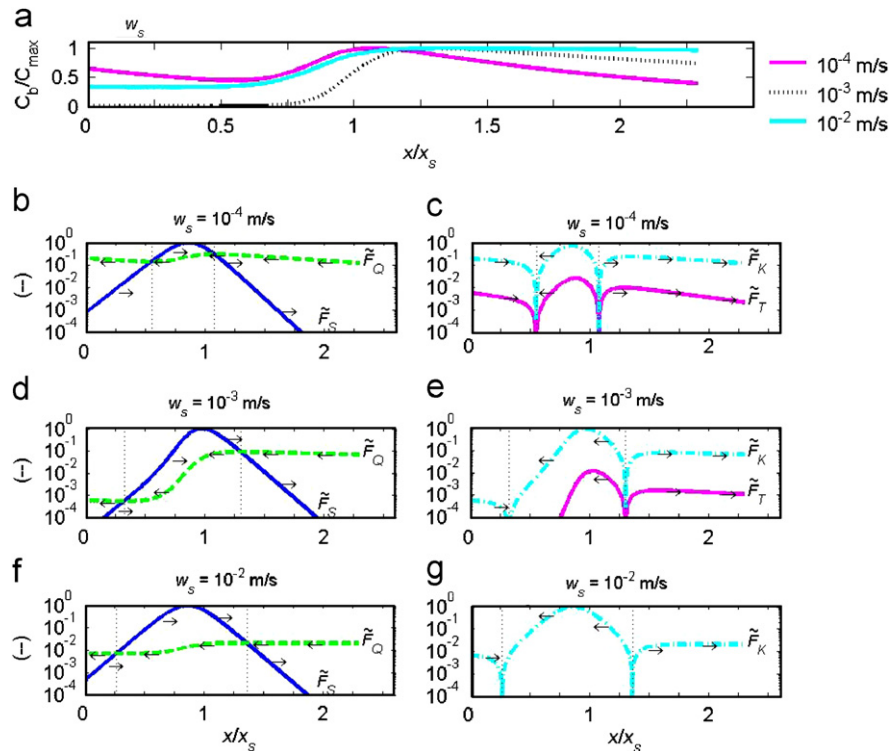
Fig. 10. Profile of normalized SSC (a) and normalized sediment transport rates (b–g) for different values of w_s, following the same format as Fig. 9. The SSC maxima for occur at $x/x_s = 1.07$, $x/x_s = 1.30$, and $x/x_s = 1.36$ for settling velocities of $w_s = 10^{-4}$, $w_s = 10^{-3}$, and $w_s = 10^{-2}$ m/s, respectively.

maximum moves upstream. The spread of SSC also varies, with the smallest spatial spread (relative to the maximum) occurring for the intermediate settling velocity of 0.001 m/s. The observed change in the spatial variation of SSC occurs because of the changing interaction of the sediment distribution (controlled by $Pe_v = w_s H/K_v$) with the (constant) circulation structure. For large settling velocity, the vertical sediment distribution shifts towards the bed and upstream currents push sediment further upstream. This results in a relative increase in transport from salinity gradients compared to freshwater discharge, and hence an upstream shift in the location of the ETM (compare Fig. 10b, d, and e). Because turbidity-gradient-driven currents decrease at large Pe_v, the relative contribution of F_T decreases as w_s increases (compare F_T in Fig. 10c and g).

For small values of settling velocity and sediment Peclet number (<1), the distribution of SSC becomes well mixed. As a consequence, sediment transport from freshwater discharge (F_Q) increases (freshwater discharge is largest at water surface), while the vertically integrated flux from salinity gradients (F_S) vanishes (because the vertically integrated gravitational circulation is zero). Hence, as shown in Fig. 10c, freshwater discharge becomes increasingly dominant as w_s and Pe_v decrease. The two limits—freshwater dominated or salinity dominated fluxes—result

in a large spread of SSC, while the intermediate case results in the smallest horizontal spread.

Fig. 11 shows the variation in longitudinal SSC that results from varying width-averaged freshwater discharge $q = Q/b$ (Fig. 11a), depth H (Fig. 11b), horizontal dispersion coefficient K_h (Fig. 11c), vertical eddy viscosity $A_v = K_v$ (Fig. 11d), the position of the maximum salinity gradient x_c (Fig. 11e), and the length scale of the salinity gradient x_L (Fig. 11f). To isolate the sensitivity of each parameter on the model, we neglect the effect that each parameter has on the others (for example, we neglect the effect of changing horizontal dispersion on the salinity field).

As width averaged freshwater discharge $q = Q/b$ (Fig. 11a) or vertical mixing ($K_v = A_v$, Fig. 11d) increase, the location of the ETM moves downstream; for large enough values, all the sediment piles up at the seaward boundary and is essentially expelled from the system (see $K_v = A_v = 0.01$ m^2/s case). The opposite trend is observed for depth: Doubling the depth from 5 m to 10 m moves the ETM far upstream, and makes the distribution of SSC highly asymmetric around its maximum. Changing the location of the maximum salinity gradient, x_c, simply shifts the SSC distribution (Fig. 11e). By contrast, increasing the salinity gradient (decreasing x_L) moves the turbidity
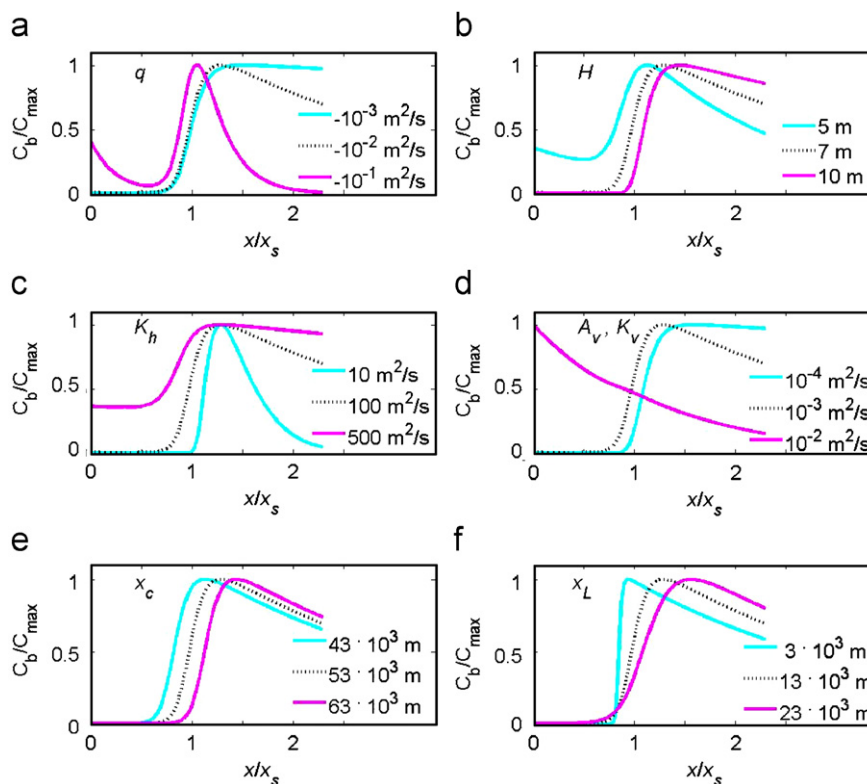

Fig. 11. Sensitivity study of freshwater discharge q (a), depth H (b), longitudinal dispersion coefficient K_h (c), eddy viscosity A_v and eddy diffusivity K_v (d), location of maximum salinity gradient x_c (e), and x_L is the length scale over which salinity varies (f). Individual parameters are varied as shown, while other parameter values are held to Table 1 defaults. In each plot, the solution using values from Table 1 is depicted with a dotted line. The x-axis is normalized by a salt intrusion length scale, $x_s = x_c + x_L \sim 65.5 \times 10^3$ m, while each profile of concentration is normalized by the concentration at its maximum. The model domain runs from $x/x_s = 0$ to $x/x_s = 2.3$.

maximum downstream and increases the gradient of SSC downstream of the maximum. As with the sensitivity study of c_*, varying the dispersion coefficient K_h only changes the distribution of SSC, but not the position. For the small value of $K_h = 10\,\mathrm{m}^2/\mathrm{s}$, it can be shown that sediment transport rates from turbidity currents (F_T) dominate over those of dispersion (F_K).

The observed variability of SSC in Fig. 11 results from changes to both the residual circulation structure and the vertical distribution of sediment. Factors that increase near-bottom currents over the model domain, such as increased depth or decreased mixing (see Eq. (12)), result in an upstream shift of sediment. An increase in surface currents (e.g., freshwater discharge) results in a down-stream shift. As occurs with settling velocity (Fig. 10), changes to the sediment Peclet number—i.e., increased depth or decreased mixing—also concentrate SSC closer to the bed and enhance the upstream movement of SSC.

The sensitivity studies in Figs. 9–11 show that the equilibrium distribution of sediment in our channel model is generally asymmetric around its maximum. This asymmetry forms because different physical mechanisms control the sediment transport balance on either side of the ETM. For the standard parameter values in Table 1, the morphodynamic equilibrium (and hence distribution of SSC) is determined primarily by a balance between sediment transport from gravitational circulation (F_S) and dispersion (F_K). Upstream of the ETM, the balance of sediment transport is formed between freshwater discharge (F_Q) and dispersion (F_K). In the sensitivity study, factors which change only F_S (e.g., x_L in Fig. 11g) only change the downstream distribution of turbidity, while factors which enter only F_Q (e.g., freshwater discharge in Fig. 11a) primarily affect the upstream distribution. Moreover, the differing effect of parameters on transport rates F_Q and F_S (e.g., see depth H in Eq. (14)) produces longitudinal asymmetry. As shown in Fig. 9, transport from turbidity currents (F_T) become increasingly important relative to dispersion (F_K) for large c_* or small K_h. Turbidity currents enhance asymmetry because they act against salinity gradients downstream of the ETM, but are oriented in the same direction upstream of the ETM.

4.2.1. Equilibrium structure of velocity

The equilibrium distribution of sediment implies an equilibrium distribution of turbidity currents for each set of model parameters. The circulation pattern resulting from the salinity gradient, the turbidity gradients, and their superposition are shown in Fig. 12 for the case of high sediment concentration ($c_* = 200\,\mathrm{kg/m}^3$). The upper panel (Fig. 12a) shows gravitational circulation driven by salinity gradients, with a landward current occurring near the bottom with a maximum of 0.04 m/s and a seaward return current near the surface with a maximum of 0.058 m/s. As the salinity gradient vanishes in the upstream direction, the gravitational circulation becomes quite small, with velocities on the order of magnitude of $10^{-4}\,\mathrm{m/s}$.
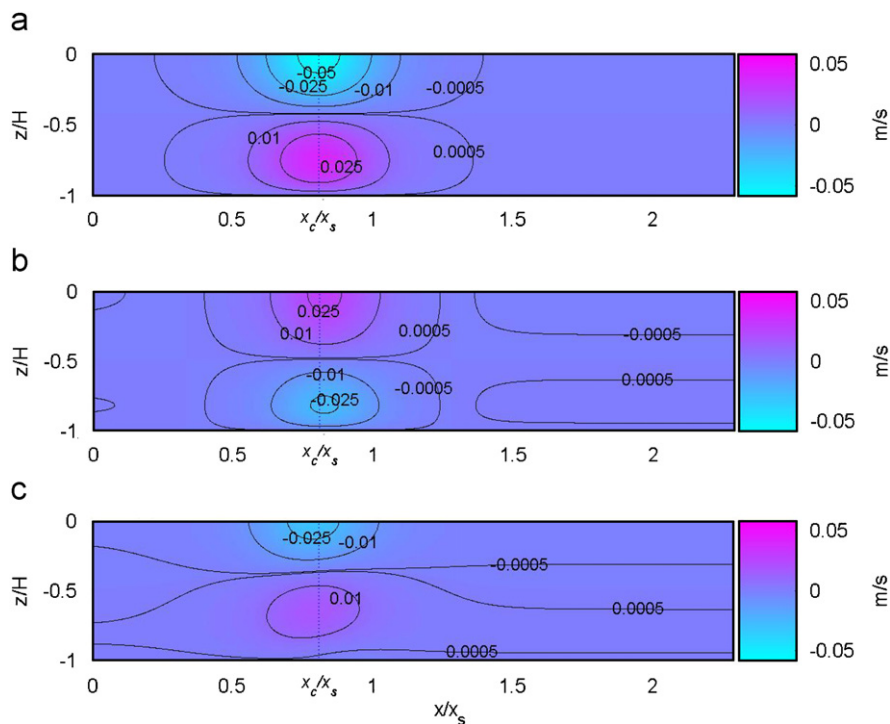

Fig. 12. Residual circulation from salinity gradients (a), turbidity gradients (b) and their combination (c) after determining an equilibrium sediment profile for an average bottom sediment concentration of $c_* = 200\,\mathrm{kg/m}^3$. For all other parameters, default values given in Table 1 are used. The x-axis is normalized by a salt intrusion length scale of $x_s = x_c + x_L \sim 65.5 \times 10^3\,\mathrm{m}$, while the vertical coordinate is normalized by $H = 7\,\mathrm{m}$. The positive direction is upstream. The location of the maximum salinity gradient, $x_c/x_s = 0.81$, is marked by a vertical dotted line.

Downstream of the turbidity maximum, turbidity currents (Fig. 12b) oppose the salinity-driven currents, with near-bottom currents heading seaward and surface currents heading landward. For the chosen c_* of 200 kg/m³, the estimated turbidity currents are the same order of magnitude, but somewhat smaller, than the salinity-gradient-induced circulation: seaward bottom currents peak at 0.027 m/s, while landward surface currents peak at 0.028 m/s. Compared to salinity-gradient-driven flow, near-bottom flow due to turbidity gradients is centered lower in the water column; however, at equilibrium, no three-layer flow is observed. The position of the maximum turbidity-driven current occurs ~1 km upstream of the maximum salinity-driven current, indicating that the maximum gradient of salinity and turbidity (which oppose each other) are nearly coincident. As a result, the combined circulation (Fig. 12c) is significantly reduced downstream of the turbidity maximum, with a peak bottom velocity of 0.018 m/s in the upstream direction. The maximum combined current is located 1400 m seaward of the maximum salinity-gradient-driven flow. Upstream of the turbidity maximum, turbidity gradients greatly enhance the upstream flow due to salinity gradients. The combined circulation is small, with a maximum of $8.8*10^{-4}$ m/s, or ~75 m per day. Over the time scales considered (order of weeks), this upstream transport can become significant.

4.3. Location of estuarine turbidity maximum

The sensitivity studies (Figs. 10 and 11) show that six model parameters (w_s, A_v, q, x_L, x_c, and depth H) alter the longitudinal position of the turbidity maximum, x_{ETM}. Applying the definition that $dC_b/dx = 0$ at the ETM, it follows from Eq. (13) that x_{ETM} is determined by sediment transport rate from the salinity gradient (F_S) and the freshwater discharge (F_Q), but not by turbidity-gradient-driven flows (F_T) or dispersive transport (F_K). Substituting the longitudinal salinity profile $s(x)$ (Eq. (6)) into Eq. (13), it follows that:

$$x_{ETM} =$$
$$x_c + x_L \tanh^{-1}\left(\left(1 + \frac{72\rho_o Q A_v T_Q}{T_S g \beta b H^4} \frac{2x_L}{S_*}\right)^{1/2}\right). \quad (15)$$

As the term in brackets approaches zero, the inverse hyperbolic tangent approaches zero (Q is negative). When the term in brackets approaches one, the inverse hyperbolic tangent approaches infinity. Within this range of values the term in brackets must operate for an ETM to exist in the model domain. Because of the $\sim 1/H^4$ dependence on depth, we expect that changes to depth will have the greatest impact in the location of the ETM. Depth, mixing, and settling velocity also enter through the ratio of T_Q/T_S, which depends on the sediment Peclet number Pe_v.

Using Eq. (15), we construct the theoretical variation of the position of the ETM vs. freshwater discharge for three
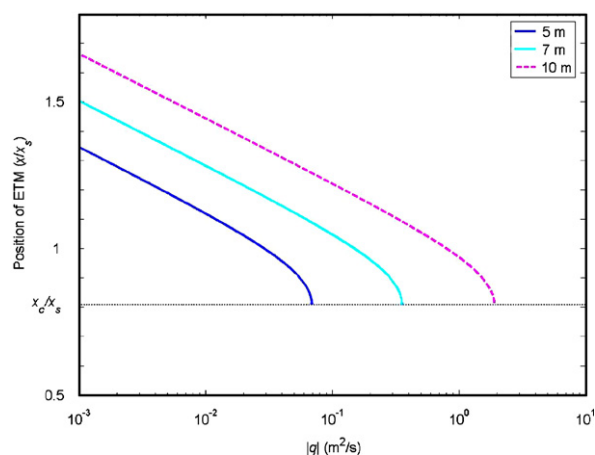

Fig. 13. Variation of the position of the estuarine turbidity maximum as a function of width averaged freshwater discharge q (m²/s) and the depth H. The standard values (Table 1) are used for all other parameters. The position of the ETM on the y-axis is normalized by a salt intrusion length scale of $x_s = x_c + x_L \sim 65.5 \times 10^3$ m. The normalized position of the maximum salinity gradient, $x_c/x_s = 0.81$, is shown with a horizontal dotted line, and is the most seaward location an ETM can form in the model.

depths ($H = 5$, 7, and 10 m; see Fig. 13). The standard values for settling velocity, eddy viscosity, and the salinity profile given in Table 1 are applied. With the exception of the high discharge limit, Fig. 13 shows that the position of the ETM varies linearly with the logarithm of freshwater discharge (for a constant salinity profile). This is a consequence of the definition of the inverse hyperbolic tangent, which is $\tanh(z) = \log((1+z)/(1-z))$. Fig. 13 also shows that the position of the ETM is strongly dependent on depth. Increasing depth from 5 to 7 m moves the ETM upstream by ~10,000 m, while deepening from 7 m to 10 m produces an additional ~10,000 m upstream migration.

As the argument in Eq. (15) approaches zero, x_{ETM} approaches the location of the maximum salinity gradient, defined by x_c (see Eq. (6)). For values less than -1, there is no real solution. Practically speaking, this means that sediment transport rates from freshwater discharge (F_Q) are larger than those from the salinity gradient (F_S) at all points in the model domain. Hence, no ETM forms and sediment is flushed out of the estuary by the freshwater discharge. Such flushing of sediment is often observed under high freshwater discharge conditions (for example, in the Seine estuary; see Le Hir et al., 2001b).

As depth is increased, the freshwater discharge Q required to push the turbidity maximum to the critical position x_c greatly increases. As Fig. 13 shows, deepening from 5 to 7 m requires freshwater discharge that is a factor of ~5 greater to reach the same position x_c. A doubling of depth from 5 to 10 m requires a factor ~27 greater freshwater discharge ($q = Qb$) before the turbidity maximum reaches x_c. For the same variation in freshwater discharge over time, the occurrence of a 'critical discharge' is therefore much less likely for a deep estuary. This is qualitatively observed in the Ems estuary, where an

upstream migration of the ETM and an increase in the suspended sediment load has been observed (e.g., Wurpts and Torn, 2005) after deepening from 5 to 7 m between 1984 and 1994. The increased accumulation of sediment after deepening is qualitatively consistent with an increased 'critical discharge' needed to export sediment out of the estuary. Because sediment cannot leave, over time sediment accumulates and SSC rises.

Because each value of the salinity gradient occurs twice, the freshwater discharge (F_Q) and salinity gradient (F_S) terms in Eq. (13) balance each other twice. Since the second derivative of the downstream balance is positive, this solution describes an estuarine turbidity minimum (see Figs. 9 and 10), or a point where the sediment transport rates from salinity gradients (F_S) and freshwater discharge (F_Q) are oriented in opposite directions. The location of the turbidity minimum, x_{min}, is described by changing the sign of the second term on the right-hand side of Eq. (15) to a minus sign. Hence, the turbidity minimum is located at the same distance downstream of the maximum salinity gradient (given by x_c) as the turbidity maximum is located upstream. Any process that moves the turbidity maximum upstream (such as decreasing flow or increasing depth) moves the turbidity minimum downstream.

5. Discussion

From the model sensitivity study (Figs. 9–11) and the analysis of the position of the turbidity maximum (Eq. (15)), we can infer the effect of changing conditions on the location and distribution of sediment. Our model predicts that the variation in eddy viscosity observed over a spring neap cycle might lead to an upstream migration of the ETM during neap tides (smaller eddy viscosity A_v). By analogy with Fig. 11, the longitudinal spread during times of reduced mixing (e.g., neap tides) should increase. Similarly, seasonal variations in settling velocity can drive variations in the location of the ETM and its trapping efficiency. For example, Sanford et al. (2001) found that particles bypassed the ETM zone of the Chesapeake during winter, but were effectively trapped during the autumn; this was attributed in an order of magnitude decrease in the median settling velocity from 0.3 (winter) to 3 mm/s (autumn). As shown in Fig. 10, our model also finds that particles with a small settling velocity are flushed out of the estuary, while heavier particles are deposited progressively further upstream. This is because larger particle sizes are distributed closer to the bottom (larger sediment Peclet number), and are moved upstream by bottom currents.

The asymmetric longitudinal profiles of SSC predicted by the model are also observed in field measurements of the Ems (see Figs. 2–4). For example, the downstream profile of surface turbidity in September 2005 is characterized by sharp gradients over ~10 km, while the upstream turbid zone is larger (~20 km) and has smaller gradients. Similarly, during low flow conditions on August 2, 2006, sediment concentrations during both the flood and ebb are asymmetrical, with a sharp decrease in SSC evident seaward of the turbid zone. Asymmetry in longitudinal SSC is also observed in the model, with the turbidity zone particularly large upstream of the ETM for low discharge or large depth (Fig. 11). The observed similarities between the model and the measurements suggest that the parameters that control the asymmetric distribution of longitudinal SSC in the model (such as sediment concentration, vertical mixing, settling velocity, longitudinal dispersion, and depth) also influence sediment distribution in a real estuary with complex bathymetry. Moreover, the model also suggests that the high sediment concentrations measured in the field produce turbidity-driven flows which feedback into the equilibrium profile of sediment (see Fig. 9). Because of the asymmetry in the longitudinal profile of SSC, the largest turbidity-driven currents generally occur downstream of the ETM, in the vicinity of the maximum longitudinal salinity gradient. The exact location of the maximum turbidity gradient (and turbidity current) is determined by the second derivative of $C_b(x)$, and hence depends on freshwater discharge as well (see Eq. (14)).

To be clear, though, the channel model is not predictive but rather gives insights into some of the physical processes occurring at the turbidity maximum. Indeed, the model neglects stratification and the tidal variation of flow and their effect on mixing, residual flow structure, and sediment fluxes. Many studies have pointed out the asymmetry in mixing that occurs in estuaries between the unstratified flood tide and the stratified ebb tide (Simpson et al., 1990; Jay and Musiak, 1994; Stacey et al., 2001). Such tidal asymmetry in mixing produces near-bottom flows that enhance residual currents from salinity gradients (Jay and Musiak, 1994; Burchard and Baumert, 1998) and alter the position of the ETM. Another source of residual circulation is the return flow caused by the correlation of tidal water level and surface velocity (e.g., Stanev et al., 2007). Bed stress asymmetry (Jay and Smith, 1990), asymmetry in eddy diffusivity (Geyer, 1993), asymmetries in tidal velocities (e.g., Allen et al., 1980), width convergence (Friedrichs et al., 1998), and settling lag and scour lag effects (Postma, 1967) drive sediment fluxes not included in our model. Flocculation processes cause the settling velocity of cohesive sediment to vary spatially and temporally, as does hindered settling at high concentrations (van der Lee, 2000; Winterwerp, 2002). Spatial variation in eddy diffusivity likely occurs due to stratification effects (Munk and Anderson, 1948) and longitudinal changes in tidal velocity. The longitudinal dispersion coefficient K_h varies with depth, freshwater discharge, and position (e.g., Monismith et al., 2002), while the salinity field depends on K_h, freshwater discharge, and likely, as suggested by this contribution, currents driven by large turbidity gradients.

These studies mentioned above show that the residual flow structure and sediment flux in estuaries is more complex than a simple balance between fresh water input,

horizontal dispersion, and gravity currents driven by salinity gradients and turbidity gradients (as our model suggests). Nonetheless, our model gives insight into the parameters that govern turbidity-gradient-driven currents and the distribution of sediment in estuarine environments and provides a starting point for including more complex, tidally varying processes.

6. Conclusions

This paper introduces a model of estuarine circulation and sediment distribution that is forced by freshwater discharge and gradients in both SSC and salinity. The model uses many of the assumptions used in the classical model of gravitational circulation by salinity gradients (Hansen and Rattray, 1965); importantly, however, sediment is not well mixed in the water column like salinity but rather is modelled as a balance between the settling velocity of sediment and the upwards diffusion by turbulence. As a consequence, the resulting vertical distribution of sediment—and hence the longitudinal gradients of sediment concentration—increase exponentially as the bed is approached. Over a tide, this exponential vertical profile is well reproduced by data from the Ems estuary (Fig. 5), and suggests that the ratio of settling velocity to eddy diffusivity (w_s/K_v) is constant in leading order. Because the longitudinal gradient in sediment concentration drives circulation, the sediment Peclet number ($Pe_v = w_s H/K_v$) controls both the vertical distribution of sediment and the magnitude and distribution of turbidity-driven currents (see Eqs. (11) and (12)). Large values of Pe_v concentrate sediment near the bed and reduce circulation, while smaller values of Pe_v elevates sediment into the water column, reducing the effect of the bed and resulting in enhanced circulation by turbidity gradients.

For estuaries with high sediment concentrations (e.g., Ems, Humber, Gironde), the model suggests that turbidity-induced currents work against salinity-induced circulation downstream of the ETM, but occur in the same direction upstream of the ETM. At high concentrations of sediment, turbidity currents are sufficient to alter the distribution of sediment along the longitudinal axis of the model, particularly in the upstream direction. When sediment concentration gradients are small, sediment transport from dispersion dominates over turbidity currents.

Many factors produce asymmetry in the longitudinal distribution of SSC, and include the salinity structure, the freshwater discharge, and other model parameters such as the depth, vertical mixing coefficient, total sediment supply, and settling velocity. Downstream of the ETM, the distribution of sediment is controlled by a balance between the upstream sediment transport from gravitational circulation (induced by salinity distribution) and the downstream sediment transport caused by turbidity-gradient-driven currents and/or horizontal dispersion. Variations to gravitational circulation and its interaction with the vertical profile of sediment (controlled by the

sediment Peclet number) cause changes to the downstream profile of SSC. The distribution of SSC upstream of the ETM is dominated by a balance between the downstream sediment transport from freshwater discharge and the upstream sediment transport from horizontal dispersion and/or turbidity currents. Variations to freshwater discharge and its interaction with the sediment Peclet number alter the upstream distribution. Increasing depth, horizontal dispersion, and settling velocity serve to increase the upstream spread of sediment, as do decreasing eddy viscosity and freshwater discharge. The differing physics controlling the spread of turbidity upstream and downstream of the turbidity maximum thus result in inherent asymmetry.

The modelled position of the turbidity maximum occurs at the convergence of vertically integrated fluxes from freshwater discharge and salinity-gradient-induced flows, and is unaffected (by definition) by turbidity-driven currents and dispersion. The position of the ETM is most sensitive to changes in depth, and it also depends on the applied salinity profile, settling velocity, eddy viscosity, and freshwater discharge. When sediment transport rates from freshwater discharge exceed those from the salinity gradient everywhere in the model domain, no solution for the ETM occurs and sediment is flushed out of the estuary. The critical value of this freshwater discharge is greatly increased as depth is increased, and suggests that deeper estuaries likely accumulate more sediment over time (given that other parameters such as salinity structure and freshwater discharge are similar).

Our model for the equilibrium distribution of sediment concentration assumes the simplest configuration possible in order to gain physical insight into the system. This process-based approach points out the fundamental aspects of turbidity-induced circulation and parameters that control the distribution of sediment. Because of its simplicity, the model is well suited for understanding the physics of ETMs and for serving as a test case against which more complex analytical and numerical models can (and should) be tested.

Appendix A

The vertical structure of currents driven by salinity gradients and turbidity gradients found in Eq. (12) are proportional to the functions k_1 and k_2, respectively, and depend on the vertical coordinate $\zeta = z/H$ and the sediment Peclet number $Pe_v = w_s H / K_v$

$$k_1(\zeta) = (1 - 9\zeta^2 - 8\zeta^3), \tag{A.1}$$

$$k_2(\zeta, Pe_v) = 12 G_1 Pe_v^{-4} \exp(-Pe_v(1 + \zeta)), \tag{A.2}$$

where G_1 is defined as

$$
\begin{aligned}
G_1 = {}& 4 Pe_v + 6\left(-1 + \frac{1}{3} Pe_v + \zeta^2 - Pe_v \zeta^2\right) \\
& \times \exp(Pe_v(1 + \zeta)) + (1 + \zeta)(6 - 6\zeta \\
& + (1 + 3\zeta) Pe_v^2) \exp(Pe_v \zeta).
\end{aligned}
\tag{A.3}
$$

The expressions T_s, T_t, T_Q, and T_K in Eqs. (13)–(15) are defined as follows:

$$T_S = -\int_{-1}^{0} k_1(\zeta) \exp\{-Pe_v(\zeta + 1)\} \, d\zeta, \tag{A.4}$$

$$T_T = \int_{-1}^{0} \{1 - \zeta^2\} \exp\{-Pe_v(\zeta + 1)\} \, d\zeta, \tag{A.5}$$

$$T_Q = -\int_{-1}^{0} k_2(\zeta, \lambda) \exp\{-Pe_v(\zeta + 1)\} \, d\zeta, \tag{A.6}$$

$$T_{K_h} = \int_{-1}^{0} \exp\{-Pe_v(\zeta + 1)\} \, d\zeta. \tag{A.7}$$

Solving, these expressions reduce to functions of the sediment Peclet number Pe_v:

$$
\begin{aligned}
T_s = {}& \frac{1}{Pe_v^4}\{(-48 + Pe_v^3 - 18 Pe_v) \exp(-Pe_v) \\
& + 48 - 30 Pe_v + 6 Pe_v^2)\}
\end{aligned}
\tag{A.8}
$$

$$T_T = 144 G_2 Pe_v^{-7} \exp(-2 Pe_v) \tag{A.9}$$

$$
\begin{aligned}
G_2 = {}& -1 + \frac{1}{12} Pe_v^4 + Pe_v^2 + \frac{1}{2} Pe_v^3 \\
& + \left(-2 Pe_v - Pe_v^2 + \frac{1}{3} Pe_v^3 + 2\right) \exp(Pe_v) \\
& + \left(-1 - Pe_v^2 + \frac{1}{6} Pe_v^3 + 2 Pe_v\right) \exp(2 Pe_v)
\end{aligned}
\tag{A.10}
$$

$$T_Q = \frac{-2}{Pe_v^3}\left\{\left(-1 + \frac{1}{2} Pe_v^2\right) \exp(-Pe_v) + 1 - Pe_v\right\} \tag{A.11}$$

$$T_{K_h} = \frac{1 - \exp(-Pe_v)}{Pe_v} \tag{A.12}$$

Appendix B. Supplementary information

Supplementary data associated with this article can be found in the online version at doi:10.1016/j.csr.2007.09.002.

References

Abril, G., Etcheber, H., Le Hir, P., Bassoullet, P., Boutier, B., Frankignoulle, M., 1999. Oxic/anoxic oscillations and organic carbon mineralization in an estuarine maximum turbidity zone (The Gironde, France). Limnology and Oceanography 44, 1304–1315.

Allen, G.P., Salomon, J.C., Bassoullet, P., Du Penhoat, Y., de Grandpre, C., 1980. Effects of tides on mixing and suspended sediment transport in macrotidal estuaries. Sedimentary Geology 26, 69–90.

Burchard, H., Baumert, H., 1998. The formation of estuarine turbidity maxima due to density effects in the salt wedge. A hydrodynamic process study. Journal of Physical Oceanography 28, 309–321.

Festa, J.F., Hansen, D.V., 1978. Turbidity maxima in partially mixed estuaries: a two dimensional numerical model. Estuarine and Coastal Marine Science 7, 347–359.

Friedrichs, C.T., Wright, L.D., 2004. Gravity-driven sediment transport on the continental shelf: implications for equilibrium profiles near river mouths. Coastal Engineering 51, 795–811.

Friedrichs, C.T., Armbrust, B.D., de Swart, H.E., 1998. Hydrodynamics and equilibrium sediment dynamics of shallow, funnel-shaped tidal estuaries. In: Dronkers, A., Scheffers, A. (Eds.), Physics of Estuaries and Coastal Seas. Balkema, Rotterdam, pp. 315–327.

Gabioux, M., Vinzon, S.B., Paiva, A.M., 2005. Tidal propagation over fluid mud layers on the Amazon shelf. Continental Shelf Research 25 (1), 113–125.

Geyer, W.R., 1993. The importance of the suppression of turbulence by stratification on the estuarine turbidity maximum. Estuaries 16 (1), 113–125.

Guan, W.B., Kot, S.C., Wolanski, E., 2005. 3-D fluid mud dynamics in the Jiaojang estuary, China. Estuarine, Coastal, and Shelf Science 65, 747–762.

van der Ham, R., Winterwerp, J.C., 2001. Turbulent exchange of fine sediments in a tidal channel in the Ems/Dollard estuary. Part II. Turbulence measurements. Continental Shelf Research 21 (15), 1605–1628.

Hansen, D.V., Rattray Jr., M., 1965. Gravitational circulation in straits and estuaries. Journal of Marine Research 23, 104–122.

Huijts, K.M.H., Schuttelaars, H.M., de Swart, H.E., Valle-Levinson, A., 2006. Lateral entrapment of sediment in tidal estuaries: an idealized model study. Journal of Geophysical Research 111, F02013.

Jay, D.A., Musiak, J.D., 1994. Particle trapping in estuarine tidal flows. Journal of Geophysical Research 99, 20,445–20,461.

Jay, D.A., Smith, J.D., 1990. Circulation, density distribution and neap-spring transitions in the Columbia River estuary. Progress in Oceanography 25, 81–112.

de Jonge, V.N., 1992. Tidal flow and residual flow in the Ems estuary. Estuarine Coastal and Shelf Science 34 (1), 1–22.

Kineke, G.C., Sternberg, R.W., 1992. Measurements of high-concentration suspended sediments using the optical backscatter sensor. Marine Geology 108 (3–4), 253–258.

Kineke, G.C., Sternberg, R.W., Trowbridge, J.H., Geyer, R.W., 1996. Fluid-mud processes on the Amazon continental shelf. Continental Shelf Research 16 (5–6), 667–696.

van der Lee, W.T.B., 2000. Temporal variation of floc size and settling velocity in the Dollard estuary. Continental Shelf Research 20, 1495–1511.

Le Hir, P., Bassoullet, P., Jestin, H., 2001a. Application of the continuous modelling concept to simulate high-concentration suspended sediment in a macrotidal estuary. In: McAnally, W.H., Mehta, A.J. (Eds.),

Coastal and Estuarine Fine Sediment Processes. Proceedings in Marine Science, Vol. 3. Elsevier Science, Amsterdam, pp. 545–561.

Le Hir, P., Ficht, A., Jacinto, R.S., Lesueur, P., Dupoint, J.P., Lafite, R., Brenon, I., Thouvenin, B., Cugier, P., 2001b. Fine sediment transport and accumulations at the mouth of the Seine estuary (France). Estuaries 24 (6B), 950–963.

Monismith, S.G., Kimmerer, W., Burau, J.R., Stacey, M.T., 2002. Structure and flow-induced variability of the subtidal salinity field in Northern San Francisco Bay. Journal of Physical Oceanography 32, 3003–3019.

Munk, W.H., Anderson, E.R., 1948. Notes on a theory of the thermocline. Journal of Marine Research 7, 276–295.

Officer, C.B., 1976. Physical oceanography of estuaries and associated coastal waters. Wiley, New York.

Parker, G., Fukushima, Y., Pantin, H.M., 1986. Self-accelerating turbidity currents. Journal of Fluid Mechanics 171, 145–181.

Postma, H., 1967. Sediment transport and sedimentation in the estuarine environment. In: Lauff, G.H. (Ed.), Estuaries. American Association of Advanced Sciences Publ. 83, Washington, DC, pp. 158–179.

Sanford, L.P., Suttles, S.E., Halka, J.P., 2001. Reconsidering the physics of the Chesapeake Bay estuarine turbidity maximum. Estuaries 24 (5), 655–669.

Scully, M.E., Friedrichs, C.T., Wright, L.D., 2002. Application of an analytical model of critically stratified gravity-driven sediment transport and deposition to observations from the Eel River continental shelf, northern California. Continental Shelf Research 22, 1951–1974.

Simpson, J.H., Brown, J., Matthew, J., Allen, G., 1990. Tidal straining, density currents, and stirring in the control of estuarine stratification. Estuaries 13, 125–132.

Stacey, M.T., Burau, J.R., Monismith, S.G., 2001. Creation of residual flows in a partially stratified estuary. Journal of Geophysical Research 106 (8), 17013–17037.

Stanev, E.V., Flemming, B.W., Bartholomä, A., Staneva, J.V., Wolff, J.O., 2007. Vertical circulation in shallow tidal inlets and back-barrier basins. Continental Shelf Research 27 (6), 798–831.

Uncles, R.J., Stephens, J.A., Harris, C., 2006. Runoff and tidal influences on the estuarine turbidity maximum of a highly turbid system: the upper Humber and Ouse Estuary, UK. Marine Geology 235, 213–228.

Winterwerp, J.C., 2001. Stratification effects by cohesive and noncohesive sediment. Journal of Geophysical Research 106 (C10), 22559–22574.

Winterwerp, J.C., 2002. On the flocculation and settling velocity of estuarine mud. Continental Shelf Research 22 (9), 1339–1360.

Wurpts, R., Torn, P., 2005. 15 years experience with fluid mud: definition of the nautical bottom with rheological parameters. Terra et Aqua 99.